A Central Scheme for Shallow Water Flows along Channels with Irregular Geometry

Jorge Balbás* and Smadar Karni†

September 24, 2007

Abstract

We present a new semi-discrete central scheme for one-dimensional shallow water flows along channels with non-uniform rectangular cross sections and bottom topography. The scheme preserves the positivity of the water height, and it is preserves steady-states of rest (i.e. it is well-balanced). Along with a detailed description of the scheme, numerous numerical examples are presented for unsteady and steady flows. Comparison with exact solutions illustrate the accuracy and robustness of the numerical algorithm.

AMS subject classification: Primary 65M99; Secondary 35L65

Key words: Hyperbolic systems of conservation and balance laws, semi-discrete schemes, Saint-Venant system of Shallow Water equations, non-oscillatory reconstructions, channels with irregular geometry.

1 The Shallow-water Model

We consider the shallow water equations along channels with non-uniform rectangular cross sections and bottom topography. The model describes flows that are nearly horizontal and can be obtained by averaging the Euler equations over the channel cross section [3], resulting in the balance law

$$\frac{\partial A}{\partial t} + \frac{\partial Q}{\partial x} = 0 \tag{1.1a}$$

$$\frac{\partial Q}{\partial t} + \frac{\partial}{\partial x}\Big(\frac{Q^2}{A} + \frac{1}{2}g\sigma h^2\Big) = \frac{1}{2}gh^2\sigma' - g\sigma hB', \tag{1.1b}$$

where h and $\sigma(x)$ are, respectively, the height of the fluid above the bottom of the channel, and the channel breadth, $A = \sigma h$ is the *wet* cross-section, $Q = Au$ is the *discharge*, with u denoting the (depth average) fluid velocity, $B(x)$ describes the bottom topography of the channel, and g is the acceleration of gravity (see figure 1.2).

1.1 Properties of the System

The system (1.1) is strictly hyperbolic for $h > 0$ and has eigenvalues

$$\lambda_1 = u - \sqrt{g\,h} \qquad \text{and} \qquad \lambda_2 = u + \sqrt{g\,h}, \tag{1.2}$$

with corresponding eigenvectors

$$\vec{e}_1 = \begin{pmatrix} 1 \\ u - \sqrt{gh} \end{pmatrix} \qquad \text{and} \qquad \vec{e}_2 = \begin{pmatrix} 1 \\ u + \sqrt{gh} \end{pmatrix}. \tag{1.3}$$

It is endowed with an entropy function

*Department of Mathematics, California State University, Northridge, CA 91330. email: jorge.balbas@csun.edu
†Department of Mathematics, University of Michigan, Ann Arbor, MI 48109. email: karni@umich.edu

$$\mathcal{E}(x,t) = \sigma h \left(\frac{1}{2} u^2 + \frac{1}{2} gh + gB \right), \tag{1.4}$$

and satisfies the entropy inequality

$$\frac{\partial \mathcal{E}}{\partial t} + \frac{\partial}{\partial x} \left[u \left(\mathcal{E} + \frac{1}{2} g \sigma h^2 \right) \right] \leq 0. \tag{1.5}$$

Smooth steady state solutions to (1.1) satisfy

$$Q = \sigma h u = Const \tag{1.6a}$$

$$E = \frac{1}{2} u^2 + g(h + B) = Const, \tag{1.6b}$$

where, for example, one readily recognizes the trivial steady state of rest

$$u(x) = 0 \qquad \text{and} \qquad w(x) = h(x) + B(x) = Const., \tag{1.7}$$

The parameters Q and E (together with the topography $B(x)$ and channel geometry $\sigma(x)$) determine the steady-state solution as the root of a nonlinear equation. A useful relation for smooth steady solutions is obtained by differentiating (1.6)

$$(1 - F^2) h_x = \frac{hF^2}{\sigma} \sigma' - B', \tag{1.8}$$

where

$$F = \frac{|u|}{\sqrt{gh}} \tag{1.9}$$

is the Froude number. Flows with Froude number $F < 1$ are said to be subcritical or *fluvial*, and flows with Froude number $F > 1$ supercritical or *torrential*. The interplay between the geometry of the channel, $\sigma(x)$, and the topography, $B(x)$, controls the flow. Equation (1.8) implies, for example, that if the crest of the topography ($B'(x) = 0$) and the throat of the channel ($\sigma'(x) = 0$) occur at the same point, then at that point either the solution is symmetric, $h_x(x) = 0$, or the flow reaches criticality, *i.e.*, $F = 1$. If the crest and throat occur at different points in the domain, the flow reaches criticality at some intermediate point where the right hand side of (1.8) vanishes.

1.2 Numerical Simulation of Shallow-water Flows

Numerical approximations of the solutions of (1.1) face numerous challenges: the system (1.1) admits discontinuous solutions, and require robust numerical schemes that are suitable for discontinuous flows.

Changes in the solution of (1.1) in time arise when flux gradients are out of balance with the geometric source terms. Numerical schemes that are able to recognize and respect such a balance often give superior results when computing near steady-state flows. Perfectly recognizing such a balance may not always be possible, and schemes that respect steady-state solutions either exactly or to the order of the numerical approximation are often called 'well-balanced'.

Another challenge arises when computing near dry-state solutions (*e.g.*, flooding or drainage flows) as system (1.1) loses strict hyperbolicity if $h = 0$. In such cases, the truncation error of the numerical scheme may cause the layer depth h to become negative, causing the computation to fail. Positivity preserving schemes have the desirable property that if the data has positive (non-negative) depth, so does the numerical solution. Positive schemes enjoy enhanced stability near dry states.

In this paper, we introduce a semi-discrete central scheme for the solution of (1.1). The scheme is second order accurate, well-balanced and positive. Nonoscillatory schemes based on central differencing offer a robust, yet simple, approach for computing the discontinuous solutions of hyperbolic problems, see for example [13, 10, 1, 2, 6, 12]. Several central schemes have been extended to handle systems with geometric source terms, in [14] Russo introduces a fully-discrete, well balance central scheme for flows along channels of constant width, and in [7, 9] several semi-discrete central schemes for one- and two-dimensional shallow water flows are presented. The central scheme described in this work extends the work in [14, 7, 9] to flows in variable geometry. The numerical

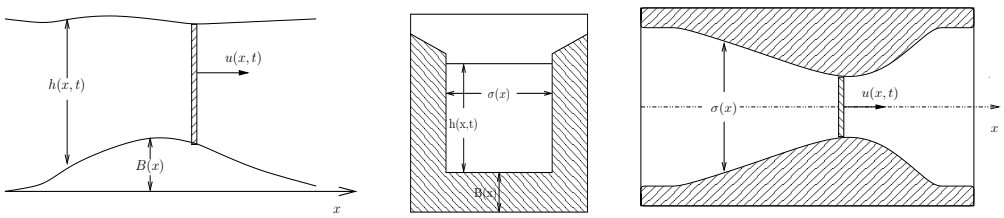

Figure 1.1: Three views of the flow. Flow profile (left), flow cross section (center) and overview of flow (right).

solutions of flows along channels of varying width have also been addressed in [17], where an upwind scheme for a hyperbolic system similar to the balance law (1.1) is proposed, and in [3] where multi-layer flows along channels with arbitrary geometries are simulated with a Q-scheme.

The proposed scheme is described in §2, and is established to preserve positivity of water height and to be well-balanced. Numerical solutions are presented in §3 for a variety of flow regimes, illustrating the scheme's accuracy and robustness and demonstrating its ability to simulate a wide range of flows.

2 A Central Scheme for One-dimensional Shallow Water Flows

In this section we construct a central scheme for the accurate simulation of shallow water flows described by the balance law (1.1). In particular, we seek a scheme that is positivity preserving and well-balanced. The scheme extends previous works in [14, 7, 9] to shallow water flows in variable geometry. This extension is not trivial; in the constant channel width model ($\sigma \equiv 1$), well-balancing may be accomplished solely by choosing an appropriate discretization of the source term. In the variable geometry case, the conserved variables σh and σhu depend on the geometry σ, which renders steady state preservation and positivity more strongly coupled with, for example, the reconstruction of the conserved variables.

Following [14], we reformulate (1.1) in terms of the total water elevation $w = h + B$ and the total area, $A^T = A + \sigma B = \sigma w$,

$$\frac{\partial A^T}{\partial t} + \frac{\partial Q}{\partial x} = 0 \tag{2.1a}$$

$$\frac{\partial Q}{\partial t} + \frac{\partial}{\partial x}\Big(\frac{Q^2}{A^T - \sigma B} + \frac{1}{2} g\,\sigma (w-B)^2\Big) = \frac{1}{2} g\sigma'(w-B)^2 - g\sigma(w-B)B'. \tag{2.1b}$$

This formulation allows the numerical scheme to detect changes (or the lack of them) in the total water elevation w, which in turn, facilitates ensuring preservation of steady states of rest.

2.1 Semi-discrete Central Formulation

We begin by describing the semi-discrete central scheme framework for approximating solutions for hyperbolic conservation laws (consult [10] and [8] for further details),

$$v_t + f(v)_x = 0. \tag{2.2}$$

For a fixed spatial scale Δx, we consider the partition of the solution domain into the grid cells $I_j := [x_j - \Delta x/2, x_j + \Delta x/2]$, and denote by $\overline{v}_j(t)$the cell average of $v(x,t)$ over the cell I_j,

$$\overline{v}_j(t) = \frac{1}{\Delta x}\int_{x_{j-\frac{1}{2}}}^{x_{j+\frac{1}{2}}} v(x,t)\,dx.$$

Integrating (2.2) over each I_j results in the equivalent semi-discrete formulation

$$\frac{d}{dt}\overline{v}_j(t) = -\frac{1}{\Delta x}\left(f(v(x_{j+\frac{1}{2}},t)) - f(v(x_{j-\frac{1}{2}},t))\right). \tag{2.3}$$

Equation (2.3) is approximated by the collection of (semi-discrete) ODEs:

$$\frac{d}{dt}\overline{v}_j(t) = -\frac{H_{j+\frac{1}{2}}(t) - H_{j-\frac{1}{2}}(t)}{\Delta x}, \tag{2.4}$$

where the flux at cell interfaces, $f(v(x_{j\pm\frac{1}{2}},t))$, is approximated by the numerical flux $H_{j\pm\frac{1}{2}}(t)$ given by

$$H_{j\pm\frac{1}{2}}(t) = \frac{f\left(v^+_{j\pm\frac{1}{2}}(t)\right) + f\left(v^-_{j\pm\frac{1}{2}}(t)\right)}{2} - \frac{a_{j\pm\frac{1}{2}}}{2}\left(v^+_{j\pm\frac{1}{2}}(t) - v^-_{j\pm\frac{1}{2}}(t)\right). \tag{2.5}$$

Here, the interface point-values of the solution, $v^{\pm}_{j\pm\frac{1}{2}}(t)$, are recovered from the cell averages $\{\overline{v}_j(t)\}$ via a non-oscillatory polynomial reconstruction $v(x,t) \approx R(x;t) = \sum_j p_j(x;t)\cdot \mathbf{1}_{I_j}$, *i.e.*,

$$v^-_{j+\frac{1}{2}} := p_j(x_{j+\frac{1}{2}}) \qquad \text{and} \qquad v^+_{j+\frac{1}{2}} := p_{j+1}(x_{j+\frac{1}{2}}), \tag{2.6}$$

and $a_{j+\frac{1}{2}}$ stands for (an estimate of) the maximum wave speed of the conservation law, (2.2), at the cell interface $x_{j+\frac{1}{2}}$, given by the spectral radius of the Jacobian matrix of $f(v)$, $\partial f/\partial v$.

This semi-discrete formulation, (2.4), and its central-upwind sequel, [8], provide a general framework for non-oscillatory central schemes, requiring for their actual implementation two ingredients: (*i*) a non-oscillatory polynomial reconstruction of the interface values $\{v^{\pm}_{j\pm\frac{1}{2}}\}_j$ from their cell averages $\{\overline{v}_j(t)\}_j$, and (*ii*) an evolution routine (*i.e.*, an ODE solver) to update these cell averages acording to (2.4).

In analogy, the semi-discrete formulation for the balance law

$$v_t + f(v)_x = S(v,x), \tag{2.7}$$

yields the semi-discrete system

$$\frac{d}{dt}\overline{v}_j(t) = -\frac{H_{j+\frac{1}{2}}(t) - H_{j-\frac{1}{2}}(t)}{\Delta x} + \frac{1}{\Delta x}\int_{x_{j-\frac{1}{2}}}^{x_{j+\frac{1}{2}}} S(v,x)\,dx. \tag{2.8}$$

For the shallow water system, 2.1,

$$v = \begin{pmatrix} A^T \\ Q \end{pmatrix} = \begin{pmatrix} \sigma w \\ \sigma(w-B)\,u \end{pmatrix}, \qquad f(v) = \begin{pmatrix} \sigma(w-B)\,u \\ \sigma(w-B)\,u^2 + \frac{1}{2}g\,\sigma(w-B)^2 \end{pmatrix}, \tag{2.9}$$

and

$$S(v,x) = \begin{pmatrix} 0 \\ \frac{1}{2}g\,\sigma'(w-B)^2 - g\sigma(w-B)B' \end{pmatrix}. \tag{2.10}$$

In addition to the non-oscillatory polynomial reconstruction and the evolution routine needed for the implementation of (2.4), the approximation of balance laws requires the discretization of the source term, $S(v,x)$, in (2.8).

2.2 Non-oscillatory Second-order Reconstruction

In order to recover the interface values $v^{\pm}_{j\pm\frac{1}{2}}(t)$ in (2.5) from the cell averages $\overline{v}_j(t)$, we employ a piece-wise linear reconstruction,

$$v(x,t) = R\left(x;\overline{u}(t)\right) := \sum_j p_j(x). \tag{2.11}$$

This reconstruction procedure is at the heart of high-resolution non-oscillatory central schemes, and requires the coefficients of the polynomials $\{p_j(x)\}$ to be determined so that $R(x;\overline{v}(t))$ satisfies the following three essential properties:

- $\mathcal{P}_1$ — Conservation of cell averages: $\overline{p}_j(x) = \overline{v}_j(t)$.

- $\mathcal{P}_2$ — Accuracy: $R(x;\overline{v}(t)) = v(x,t) + \mathcal{O}((\Delta x)^2)$.
- $\mathcal{P}_3$ — Non-oscillatory behavior of $\sum_j p_j(x)$.

For the shallow water system, (2.1) we also require that the reconstructed values of the total area, A^T, and the corresponding values of the total water height, w, satisfy the following properties:

- $\mathcal{P}_4$ — Flux gradient and source balancing: for steady-sates of rest, the interface values of the water height, h, must satisfy
$$h^-_{j+\frac{1}{2}} - h^+_{j-\frac{1}{2}} = -(B(x_{j+\frac{1}{2}}) - B(x_{j-\frac{1}{2}})). \tag{2.12}$$
- $\mathcal{P}_5$ —Positivity: the reconstructed values $w^{\pm}_{j\pm\frac{1}{2}}(t)$ must yield $h^{\pm}_{j\pm\frac{1}{2}}(t) \geq 0$, so as to ensure the positivity of $\overline{h}_j(t+\Delta t)$.

2.2.1 Minmod Reconstruction: Properties $\mathcal{P}_1$ - $\mathcal{P}_3$

To guarantee properties $\mathcal{P}_1$–$\mathcal{P}_3$, we employ a second-order *minmod* reconstruction, [16, 5]. The total area, A^T, and the discharge, Q, are reconstructed from their cell averages as the piecewise linear functions (the reconstruction is applied to values at time t, thus we can avoid the explicit reference to the time variable for its description)

$$p_j(x) = \overline{v}_j + v'_j(x - x_j), \tag{2.13}$$

with the slopes v'_j calculated as

$$v'_j = \frac{1}{\Delta x}\text{minmod}\left(\alpha\Delta_-\overline{v}_j,\, \Delta_0\overline{v}_j,\, \alpha\Delta_+\overline{v}_j\right), \tag{2.14}$$

where $1 \leq \alpha < 2$, and

$$\text{minmod}(x_1, x_2, x_3, \ldots, x_k) = \begin{cases} \min_j(x_j) & \text{if} \quad x_j > 0 \quad \forall\, j \\ \max_j(x_j) & \text{if} \quad x_j < 0 \quad \forall\, j \\ 0 & \text{otherwise} \end{cases}. \tag{2.15}$$

2.2.2 Reconstruction of Height: Properties $\mathcal{P}_4$ and $\mathcal{P}_5$

In order to enforce property $\mathcal{P}_4$ and obtain a well-balanced scheme, we first recover the cell averages of w from those of A^T as

$$\overline{w}_j := \frac{\overline{A}^T_j}{\sigma_j}. \tag{2.16}$$

For the flows calculated in §3 below, the initial conditions are given for u (or Q) and w, allowing us to define $\overline{A}^T_j := \sigma(x_j)\overline{w}_j$. Other values can be chosen within the second order accuracy of the scheme (*e.g.*, $\sigma_j = \overline{\sigma}_j$).

The interface values $w^{\mp}_{j\pm\frac{1}{2}}$ are then obtained using the minmod reconstruction (2.13) - (2.15).

To ensure the positivity of $h^{\mp}_{j\pm\frac{1}{2}}$, we follow [9], and limit the slope of the reconstructed values of w as follows (see figure 2.1):

$$\begin{aligned} &\text{if} \quad w^+_{j-\frac{1}{2}} < B(x_{j-\frac{1}{2}}), \qquad \text{then set} \qquad w'_j := 2(\overline{w}_j - B(x_{j-\frac{1}{2}})), \\ &\Rightarrow \quad w^+_{j-\frac{1}{2}} = B(x_{j-\frac{1}{2}}), \qquad \text{and} \qquad w^-_{j+\frac{1}{2}} = \overline{w}_j + \frac{1}{2}w'_j, \end{aligned} \tag{2.17}$$

or

$$\begin{aligned} &\text{if} \quad w^-_{j+\frac{1}{2}} < B(x_{j+\frac{1}{2}}), \qquad \text{then set} \qquad w'_j := 2(B(x_{j+\frac{1}{2}}) - \overline{w}_j), \\ &\Rightarrow \quad w^-_{j+\frac{1}{2}} = B(x_{j+\frac{1}{2}}), \qquad \text{and} \qquad w^+_{j-\frac{1}{2}} = \overline{w}_j - \frac{1}{2}w'_j, \end{aligned} \tag{2.18}$$

This linear reconstruction of w clearly satisfies property $\mathcal{P}_5$, $w^{\pm}_{j+\frac{1}{2}} \geq B(x_{j+\frac{1}{2}})$, which in turn will guarantee the positivity of $\overline{h}_j(t+\Delta t)$, whose interface values are defined as

$$\begin{aligned} h^-_{j+\frac{1}{2}} &:= w^-_{j+\frac{1}{2}} - B(x_{j+\frac{1}{2}}) \\ h^+_{j-\frac{1}{2}} &:= w^+_{j-\frac{1}{2}} - B(x_{j-\frac{1}{2}}), \end{aligned} \tag{2.19}$$

which satisfy (2.12) when $w^+_{j-\frac{1}{2}} = w^-_{j+\frac{1}{2}} = w$ as required for well balance.

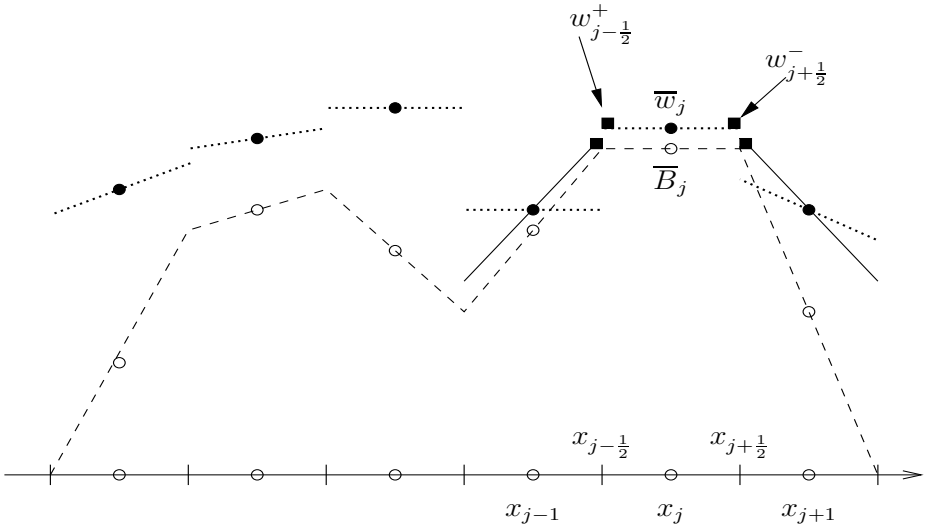

Figure 2.1: Modified reconstruction of total water height, w, over the piecewise linear approximation of bottom topography (dashed line). The minmod reconstruction is depicted by dotted lines over cell averages (black dots), the modified reconstruction is depicted by a black solid line, the interface pointvalues of w, $w_{j\pm\frac{1}{2}}$, are depicted by black squares.

2.3 Balance: Discretization of the Source Term and Preservation of Steady State

In the context of shallow water systems, a useful guiding principle in the discretization of the source term in (1.1b) and its cell average in (2.8) is that the resulting scheme is able to recognize and respect steady state solutions. Analytically, such solutions are characterized by a perfect balance between the flux gradient and the source term. Ideally, this property should be inherited by the scheme. In practice, a discrete perfect balance may not be possible to achieve for general steady states, the following discretization respects steady states of rest exactly and more general steady states are respected to the order of the numerical approximation.

For steady states of rest ($u = 0,\ h + B = const$), the second component of the numerical flux in (2.8) reduces to

$$H_{j\pm\frac{1}{2}}(t) = \frac{f\big(v^+_{j\pm\frac{1}{2}}\big) + f\big(v^-_{j\pm\frac{1}{2}}\big)}{2} = f\big(v_{j\pm\frac{1}{2}}\big) = \frac{1}{2}\, g\, \sigma_{j\pm\frac{1}{2}} h^2_{j\pm\frac{1}{2}}. \tag{2.20}$$

and the flux difference term in (2.8) reads

$$-\frac{H_{j+\frac{1}{2}}(t) - H_{j-\frac{1}{2}}(t)}{\Delta x} = \frac{g}{2\,\Delta x}\,\Big(\sigma_{j+\frac{1}{2}} h^2_{j+\frac{1}{2}}(t) - \sigma_{j-\frac{1}{2}} h^2_{j-\frac{1}{2}}(t)\Big). \tag{2.21}$$

We write the right hand side of (2.21) as

$$\frac{g}{2\,\Delta x}\left(\sigma_{j+\frac{1}{2}}h^2_{j+\frac{1}{2}}-\sigma_{j-\frac{1}{2}}h^2_{j-\frac{1}{2}}\right)= \\ \frac{g}{2\,\Delta x}\left[\frac{1}{2}\left(\sigma_{j+\frac{1}{2}}-\sigma_{j-\frac{1}{2}}\right)\left(h^2_{j+\frac{1}{2}}+h^2_{j-\frac{1}{2}}\right)+\frac{1}{2}\left(\sigma_{j+\frac{1}{2}}+\sigma_{j-\frac{1}{2}}\right)\left(h^2_{j+\frac{1}{2}}-h^2_{j-\frac{1}{2}}\right)\right]. \tag{2.22}$$

And, in view of this, discretize the cell average of the source term, (2.10), with the approximations

$$\frac{g}{\Delta x}\int_{x_{j-\frac{1}{2}}}^{x_{j+\frac{1}{2}}}\frac{1}{2}\sigma'\,h^2\,dx\approx\frac{g}{2}\,\frac{\sigma_{j+\frac{1}{2}}-\sigma_{j-\frac{1}{2}}}{\Delta x}\cdot\frac{(h^-_{j+\frac{1}{2}})^2+(h^+_{j-\frac{1}{2}})^2}{2}, \tag{2.23}$$

and

$$-\frac{g}{\Delta x}\int_{x_{j-\frac{1}{2}}}^{x_{j+\frac{1}{2}}}\sigma\,h\,B'\,dx\quad\approx\quad-g\,\frac{\sigma_{j+\frac{1}{2}}+\sigma_{j-\frac{1}{2}}}{2}\cdot\frac{h^-_{j+\frac{1}{2}}+h^+_{j-\frac{1}{2}}}{2}\cdot\frac{B(x_{j+\frac{1}{2}})-B(x_{j-\frac{1}{2}})}{\Delta x}. \tag{2.24}$$

We observe that the approximation (2.23) exactly balances the first product on the right hand side of (2.22) and, with the interface pointvalues of the water height reconstructed as (2.19), (2.24) exactly balances the second product on the right hand side of (2.22). With this discretization, the right hand side (RHS) of the momentum balance in (2.8) vanishes for steady state of rest.

To ensure preservation of total water height w remains constant over time, *i.e.*, the first component of the numerical fluxes, $H_{j\pm\frac{1}{2}}$, must be calculated so that their difference yields

$$\frac{d\overline{A}^T_j}{dt}=0 \tag{2.25}$$

when $w=Const.$ and $u\equiv 0$.

We approximate the interface jump of the total area in the numerical flux of the total area in (2.8) by

$$A^{T,+}_{j+\frac{1}{2}}-A^{T,-}_{j+\frac{1}{2}}\equiv\sigma(x_{j+\frac{1}{2}})(w(x^+_{j+\frac{1}{2}},t)-w(x^-_{j+\frac{1}{2}},t))\approx\sigma_{j+\frac{1}{2}}(w^+_{j+\frac{1}{2}}-w^-_{j+\frac{1}{2}}), \tag{2.26}$$

where

$$\sigma_{j+\frac{1}{2}}=\max\{\sigma^-_{j+\frac{1}{2}},\sigma^+_{j+\frac{1}{2}}\}, \tag{2.27}$$

with

$$\sigma^-_{j+\frac{1}{2}}:=\frac{A^{T,-}_{j+\frac{1}{2}}}{w^-_{j+\frac{1}{2}}}\qquad\text{and}\qquad\sigma^+_{j+\frac{1}{2}}:=\frac{A^{T,+}_{j+\frac{1}{2}}}{w^+_{j+\frac{1}{2}}}. \tag{2.28}$$

Remarks:

1. Approximating $A^{T,+}_{j+\frac{1}{2}}-A^{T,-}_{j+\frac{1}{2}}$ by (2.26) ensures that this term vanishes for steady states of rest as required.
2. The choice of $\sigma_{j\pm\frac{1}{2}}$ in (2.26) ensures positive values of the cell average of the water height $\overline{h}_j(t+\Delta t)$ (see appendix A); other choices are possible within the second order accuracy of the scheme.

2.4 Time Evolution

Given the reconstructed interface values at time t as described in §2.2,

$$v^\pm_{j\pm\frac{1}{2}}(t)=\begin{pmatrix}A^\pm_{j\pm\frac{1}{2}}(t)\\ \\ Q^\pm_{j\pm\frac{1}{2}}(t)\end{pmatrix}, \tag{2.29}$$

we estimate the maximum interface wave speeds of (2.1) as

$$a_{j\pm\frac{1}{2}}=\max\left\{|u^-_{j\pm\frac{1}{2}}|+\sqrt{gh^-_{j\pm\frac{1}{2}}},\ |u^+_{j\pm\frac{1}{2}}|+\sqrt{gh^+_{j\pm\frac{1}{2}}}\right\}, \tag{2.30}$$

and the ODE system (2.8) is numerically integrated using the second order *Strong Stability Preserving* Runge-Kutta scheme, [15, 4],

$$\begin{aligned} v^{(1)} &= v^{(0)} \quad + \quad \Delta t\, C[v^{(0)}], \\ v^{(2)} &= v^{(1)} \quad + \quad \frac{\Delta t}{2}\left(C[v^{(1)}] + C[v^{(0)}]\right), \\ \overline{v}(t+\Delta t) &:= \quad v^{(2)}, \end{aligned} \tag{2.31}$$

with the numerical fluxes

$$C[v(t)] = -\frac{H_{j+\frac{1}{2}}(v(t)) - H_{j-\frac{1}{2}}(v(t))}{\Delta x} + \overline{S}_j(t) \tag{2.32}$$

where $H_{j\pm\frac{1}{2}}$ is given by (2.5), using (2.26), and the cell average of the source term, $\overline{S}_j$, approximated by (2.23) – (2.24).

2.5 Properties of the Scheme and Additional Remarks

To conclude this section, we summarize the two main properties of the semi-discrete central scheme resulting from applying the discretization of the source term (2.23) – (2.24), along with the reconstruction (2.13) – (2.19), and the SSP Runge-Kutta solver (2.31) – (2.32) to the semi-discrete central formulation (2.8). (We defer the proofs of the following theorems to appendix A).

Theorem 2.1 *Consider the balance law* (2.1) *and the semi-discrete central formulation* (2.8) *with the spatial integral of the source term approximated by* (2.23) – (2.24)*, the interface pointvalues of* $w(x,t)$ *and* $h(x,t)$*, given respectively by* (2.17) – (2.18) *and* (2.19)*, those of* $A^T(x,t)$*,* $Q(x,t)$ *recovered by the minmod reconstruction* (2.13) – (2.15)*, and the jump of the total area across the cell interfaces approximated by* (2.26) – (2.27)*. Then*

(*i*) *the system of ODEs* (2.8) *satisfies*

$$\frac{d}{dt}\begin{pmatrix} \overline{A}_j^T(t) \\ \overline{Q}_j(t) \end{pmatrix} = 0 \qquad \forall\, j, \tag{2.33}$$

for $w = Const.$ *and* $u \equiv 0$*, i.e., the central scheme is well-balanced, and*

(*ii*) *if the cell averages* $\overline{A}^T(t)$ *are such that*

$$\overline{w}_j(t) - \frac{1}{2}\left(B(x_{j-\frac{1}{2}}) + B(x_{j+\frac{1}{2}})\right) \geq 0, \qquad \forall\, j, \tag{2.34}$$

then, the cell averages $\overline{A}^T(t+\Delta t)$ *as evolved with* (2.31) – (2.32) *under the* CFL *limitation,*

$$\frac{\Delta t}{\Delta x} < \frac{\sigma_j}{2a_j} \quad \forall j, \tag{2.35}$$

where $a_j = \max\{a_{j-\frac{1}{2}}\sigma_{j-\frac{1}{2}},\ a_{j+\frac{1}{2}}\sigma_{j+\frac{1}{2}}\}$*, will yield*

$$\overline{w}_j(t+\Delta t) - \frac{1}{2}\left(B(x_{j-\frac{1}{2}}) + B(x_{j+\frac{1}{2}})\right) \geq 0, \qquad \forall\, j. \tag{2.36}$$

The fluxes f in (2.9) require the pointwise values of the flow velocity $u^{\mp}_{j\pm\frac{1}{2}}$. Recovering the flow velocity via Q/A may be inaccurate when h (hence both Q and A) is very small, and may lead to instabilities. To prevent this, we follow the de-singularization strategy proposed in [9], and compute the flow velocity, u, according to

$$u = \frac{\sqrt{2}AQ}{\sqrt{A^4 + \max(A^4, \epsilon)}}, \tag{2.37}$$

with $\epsilon = (\Delta x)^4$, and recalculate the discharge $Q := A \cdot u$ accordingly. When A is small, we must recalculate the discharge as $Q := A \cdot u$ so as to ensure the well balance and positivity properties (consult [9] for a detailed discussion of this and other desingularization techniques).

3 Numerical Results

In this section we present the numerical solutions for a range of problems illustrating the properties of our central scheme in a variety of flow situations: we validate the ability of the scheme to respect steady states of rest (1.7), and study its ability to propagate small perturbations from rest. The positivity of the scheme is demonstrated by solving several so-called *dam-break* problems, where a reservoir initially at rest drains through its boundaries. Finally, we study the convergence of transient solutions to more general steady state solutions by comparing them to the exact solutions. As pointed out in §2.5, exact steady state solutions are available. These are determined by the parameters Q and E, and are obtained by iterative root finding of (1.6) (*e.g.*, using Newton's method).

The flows are calculated along channels with varying width, we have used channels with a parabolic contraction. The contraction is described by the quadratic interpolant through the points $(x_l, 1)$, $(\frac{1}{2}(x_l + x_r), \sigma_{min})$, and $(x_r, 1)$, where x_l, and x_r are, respectively, the left and right end-points of the contraction along the x-axis, and σ_{min} stands for the minimum width of the channel (with $\sigma_{min} = 1$ corresponding to a straight channel).

For all the results presented below the value of the acceleration of gravity is taken as $g = 9.81$, and the time step, Δt, satisfies the CFL restriction

$$\Delta t \leq \frac{c\,\Delta x}{\max_j a_{j+\frac{1}{2}}}, \qquad c < 1. \tag{3.1}$$

Unless otherwise mentioned, the computations below were performed using 200 grid cells and $c = 0.75$.

3.1 Steady-state of Rest and Small Perturbation from Rest

3.1.1 The Steady-state of Rest

For this problem, the initial conditions correspond to the equilibrium solution,

$$w(x,0) = 1 \qquad \text{and} \qquad u(x,0) = 0, \tag{3.2}$$

with the bottom topography given by

$$B(x) = \begin{cases} \frac{1}{4}\left(1 + \cos\frac{\pi(x-0.5)}{0.1}\right) & \text{if} \quad x \in [0.4, 0.6] \\ 0 & \text{otherwise} \end{cases}. \tag{3.3}$$

Computed solutions are shown in figure 3.1 for different channel geometries. Three cases are shown. In all cases, the topography crest is centered at $x = 0.5$. In the middle example, the contraction is also centered at $x = 0.5$, in the case on the left, the throat slightly precedes the crest, while on the right, the throat is slightly after the crest (see top figures respectively). The steady state of rest is clearly respected by the scheme.

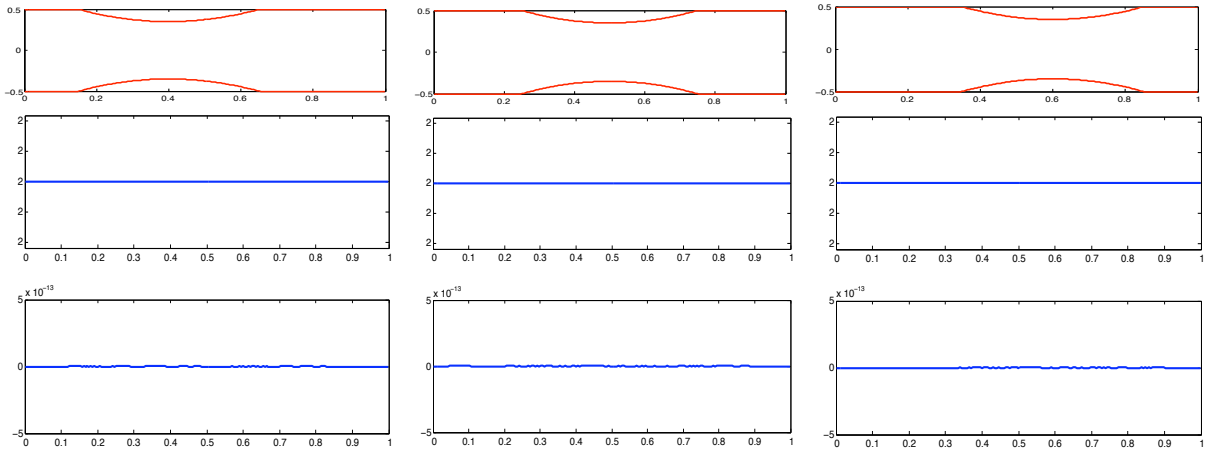

Figure 3.1: Computation of steady-state of rest through contracting channels. Top: channel longitudinal shape ($\sigma_{min} = 0.7$ in all cases), middle: total water heigh, w, bottom: Flow velocity, u.

3.1.2 Small Perturbations from Rest

For the following problems, the initial conditions correspond to a small perturbation of the steady state of rest,

$$u(x,0) = 0 \qquad \text{and} \qquad w(x,0) = \begin{cases} 1+\epsilon & \text{if} \quad 0.1 \leq x \leq 0.2 \\ 1 & \text{otherwise} \end{cases} . \tag{3.4}$$

Figure 3.2 shows the initial conditions and several snapshots of the perturbation as it propagates for the case $\epsilon = 10^{-2}$. Figure 3.3 shows the solution at $t = 0.4$ with $\epsilon = 10^{-5}$ for a channel with a centered contraction. Numerical methods that do not respect steady state of rest have hard time computing accurately the propagation of perturbations of this small magnitude, [11]. As can be observed, the perturbation is propagated accurately by the numerical scheme.

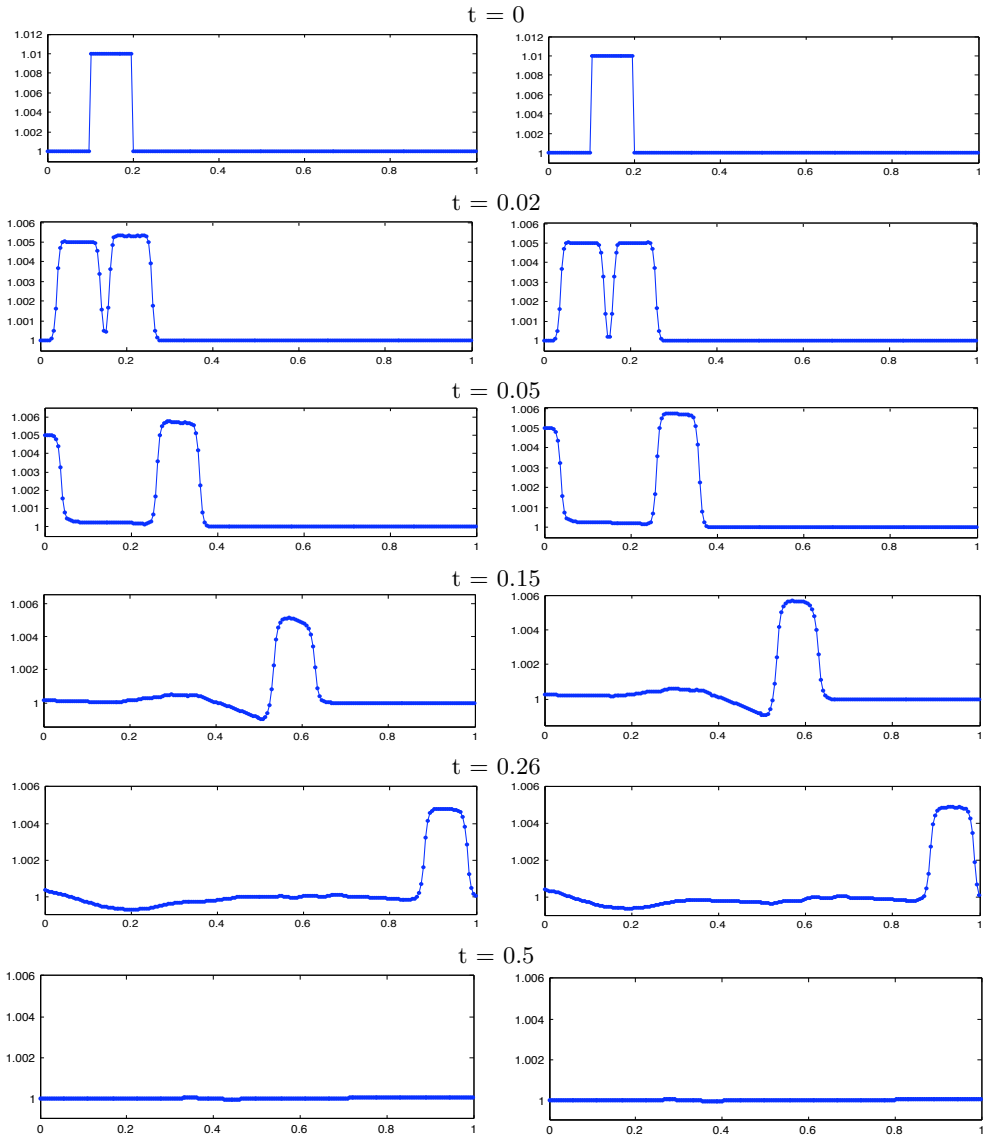

Figure 3.2: Propagation of small disturbances from rest (3.4) through contracting channels, $\epsilon = 10^{-2}$, using CFL number (3.1) with $c = 0.65$. Left: a channel with a left shifted contraction, right: a channel with a centered contraction.

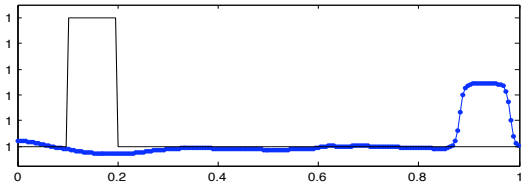

Figure 3.3: Propagation of small disturbances from rest, (3.4) through contracting channels, $\epsilon = 10^{-5}$, using CFL number (3.1) with $c = 0.65$. Total water height, w, at $t = 0.26$ (dots) over initial conditions (solid line).

3.2 Dam Break Problems

In this problem, we consider a (symmetric) reservoir initially at rest, draining onto a dry bed through its boundaries, leaving behind water trapped in topographical troughs. Due to the symmetry, the flow is computed on half the domain, with open boundary conditions on the right boundary, and reflecting bc's on the left boundary. This flow is computationally challenging as water depth h becomes increasingly small due to drainage, and may lead to breakdown of the solution if water depth becomes negative due to numerical error. The positivity property of the scheme insures the water depth remains non-negative. Two bottom topographies are considered, consisting of one or two topographical *bumps*. The initial conditions are, in both cases,

$$u(x, 0) = 0, \qquad \text{and} \qquad w(x, 0) = 0.8. \tag{3.5}$$

At outflow, the boundary conditions are implemented as follows: if the flow is supercritical, both w and Q are extrapolated from the interior of the domain, while if the flow is subcritical, the water height h_{out} is prescribed to dry bed, $h = 0$ - in fact we have used $h_{out} = 10^{-16}$– and Q is extrapolated. Solution snapshots are presented in Figures 3.4, **??**, and 3.5.

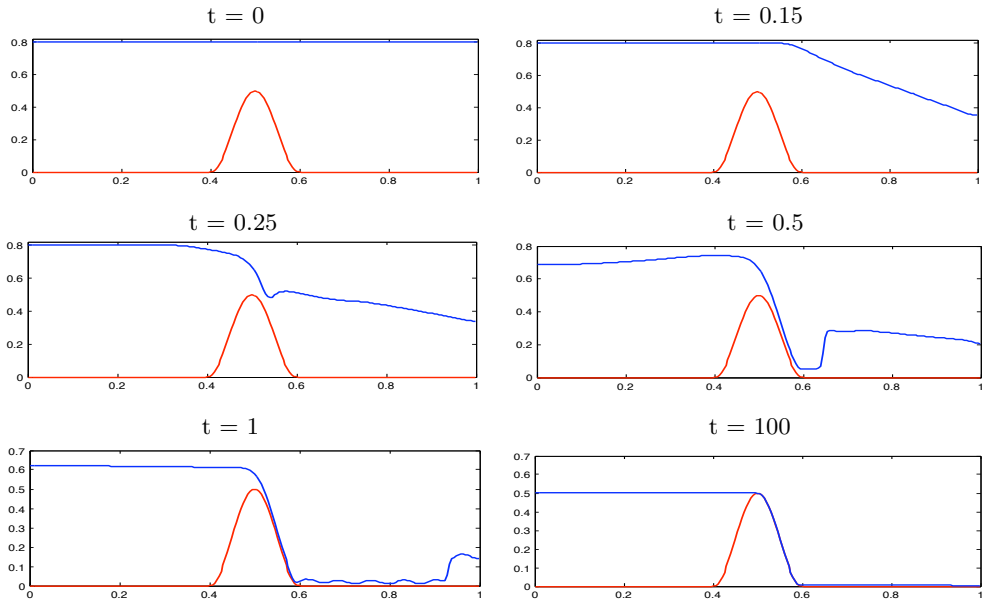

Figure 3.4: Dam break and drainage through a contracting channel: initial conditions (3.5), crest and throat coincide $\sigma'(0.5) = B'(0.5) = 0$. Total water elevation, w, at various times.

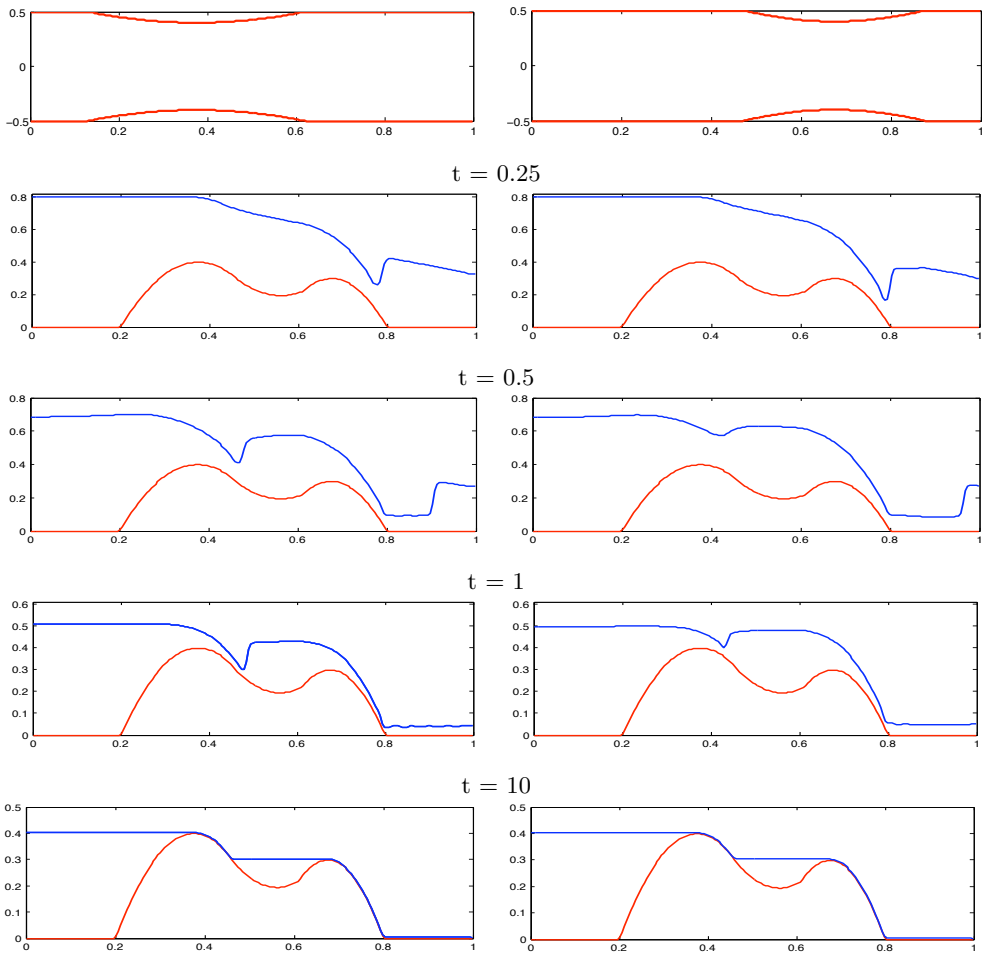

Figure 3.5: Dam break and drainage through a contracting channel with initial conditions (3.5). Left: throat coincides with left crest $\sigma'(0.325) = B'(0.325) = 0$. Right: throat coincides with right crest, $\sigma'(0.675) = B'(0.675) = 0$. Total water elevation, w, is shown at various times.

3.3 Non-trivial Steady-states

In this section we compute general steady states by integrating the time dependent equations (1.6) for very long time until steady state is reached. The computed solutions are compared with exact steady state solutions. We study various channel configurations, and compare flows in a straight channel to flows in contracting channels. We present computed solutions for a subcritical flow, for a smooth transcritical flow, and for a non-smooth transcritical flow.

For the flows considered here, we consider the solution domain $x \in [-10, 10]$, along channels with parabolic contractions as those described above, and with the bottom topography given by

$$B(x) = \max\{0.2 - 0.05\, x^2, 0\} \tag{3.6}$$

The boundary conditions for these steady flows are calculated according to the eigen values of the system, (1.2): at the (left) inflow boundary, the values of Q and A^T are extrapolated from the interior of the domain if both eigen values are negative, the value of Q is prescribed and that of A^T extrapolated if $\lambda_1 < 0$ and $\lambda_2 > 0$, and both quantities are prescribed if both eigen values are positive. Correspondingly, at the outflow (right) boundary both values are extrapolated when the eigen values are both positive, prescribed when both eigen values are negative, and one is prescribed (h_{out} in this case) and one extrapolated (Q) if they have opposite signs.

3.3.1 Subcritical Smooth Flow

For this flow, we take as initial conditions

$$w(x,0) = 2, \qquad \text{and} \qquad Q(x,0) = 4.42, \tag{3.7}$$

and compute the solution along a channel with a centered contraction (*i.e.*, $\sigma'(0) = B'(0) = 0$). The flow will remain subcritical provided the channel contraction is not too severe ($\sigma_{min} > 0.8842$).

The computed large time solutions together with the exact solutions are displayed in Figure 3.6. To get a sense of the effect of channel contraction on the flow, the solution is also computed in a straight channel. Also shown are the computed solutions for the parameters Q and E, the exact values of which are constant in the steady limit. We note that the computed values of Q and E are constant within less than 0.21% and 0.13% respectively in the computed solution.

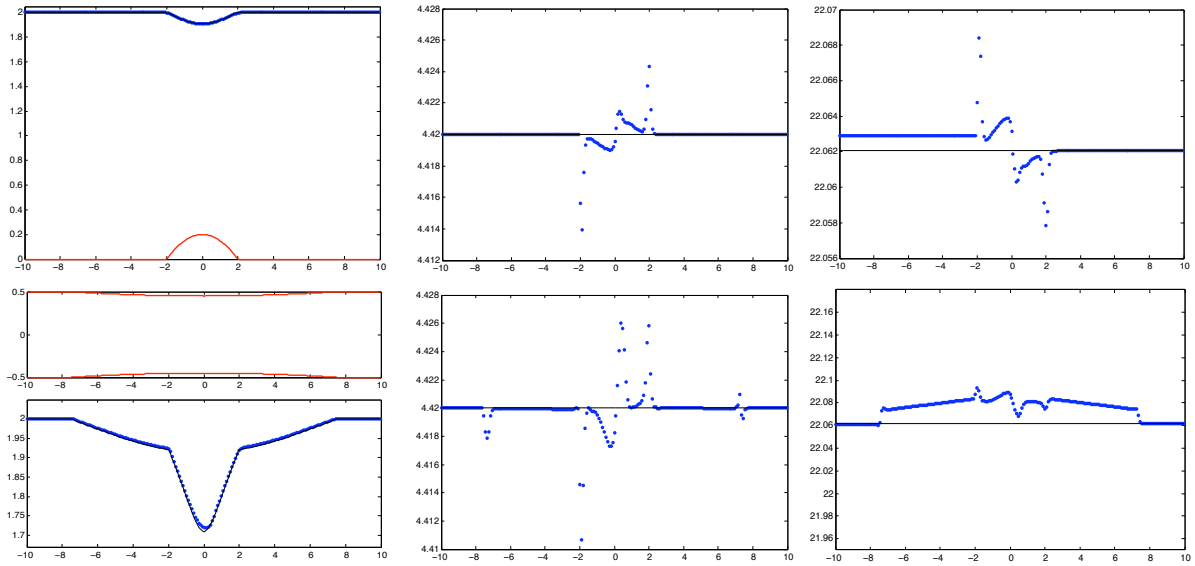

Figure 3.6: Smooth (subcritical) steady-state flow. Top: straight channel ($\sigma \equiv 1$), bottom: varying channel ($\sigma_{min} = 0.9$). Computed solution (dots) and exact equilibrium solution (solid line). Left: total water elevation, $w = h + B$ and channel geometry, center: discharge, $Q = \sigma hu$, right: total energy, E.

3.3.2 Transcritical Smooth Flow

The steady state solutions in the following examples correspond to flows accelerating smoothly from subcritical ($F < 1$) to supercritical ($F > 1$) through channels with a 30% contraction. The flow reaches criticality as it runs over the bump and through the contraction at a point between the throat of the channel and the crest of the topography.

For these flows, we take as initial conditions

$$w(x,0) = \begin{cases} 1.31 & \text{if } x < 0 \\ 0.34 & \text{if } x > 0 \end{cases} \qquad \text{and} \quad Q(x,0) = 1.53. \tag{3.8}$$

Figure 3.7 displays the computed and exact steady state solutions. For this problem, we have used a CFL number $c = 0.6$. Computed values of Q and E are constant within 1.8%.

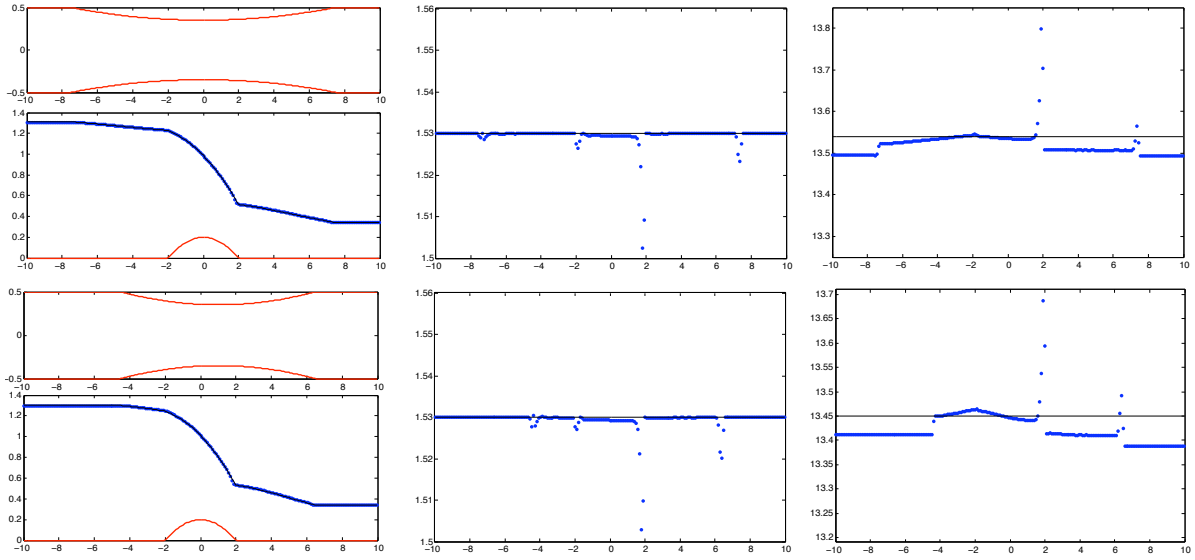

Figure 3.7: Smooth transcritical steady-state flow in a contracting channel ($\sigma_{min} = 0.7$), computed solution (dots) and exact solution (solid line). Top: channel with centered contraction, bottom: channel with right-shifted contraction. Left: total water elevation, $w = h + B$, and channel geometry, center: discharge $Q = \sigma hu$, right: flow energy E.

3.3.3 Transcritical Flow with a Shock

In this example the initial conditions are again (3.7) but the channel has narrower contraction than those considered in the subcritical case ($\sigma_{min} < 0.8842$). The steady state solution corresponds to a flow accelerating from sub- to supercritical as it runs over the bump and through the contraction, then decelerates abruptly to subcritical flow through a shock (hydraulic jump) in order to match the outflow boundary conditions. Solutions corresponding to a centered contraction and a left-shifted contraction are presented in figure 3.8. The computed values of Q and E are, respectively, within 4.0% and 3.7% of the corresponding (piecewise) constant values.

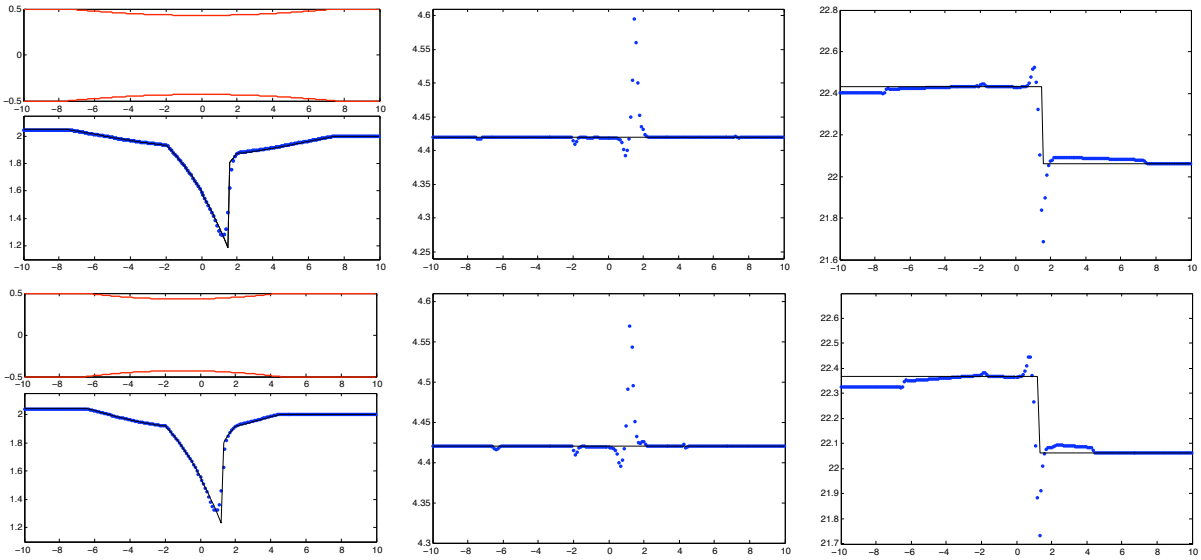

Figure 3.8: Transcritical steady-state flow in a contracting channel ($\sigma_{min} = 0.86$), computed solution (dots) and exact solution (solid line). Top: channel with centered contraction, bottom: channel with left-shifted contraction. Left: total water elevation, $w = h + B$, and contraction, center: discharge $Q = \sigma hu$, right: flow energy E.

Acknowledgment: Work supported in part by NSF, Award number DMS 0609766. The authors would like to thank Alfredo N. Wetzel (Department of Mathematics and Aerospace Engineering, University of Michigan) for helping us compute exact solutions.

References

[1] Jorge Balbás and Eitan Tadmor. Nonoscillatory central schemes for one- and two-dimensional magnetohydrodynamics equations. ii: High-order semidiscrete schemes. SIAM Journal on Scientific Computing, 28(2):533–560, 2006.

[2] Jorge Balbás, Eitan Tadmor, and Cheng-Chin Wu. Non-oscillatory central schemes for one- and two-dimensional MHD equations. I. J. Comput. Phys., 201(1):261–285, 2004.

[3] Manuel J. Castro, José A. García-Rodríguez, José M. González-Vida, Jorge Macías, Carlos Parés, and M. Elena Vázquez-Cendón. Numerical simulation of two-layer shallow water flows through channels with irregular geometry. J. Comput. Phys., 195(1):202–235, 2004.

[4] Sigal Gottlieb, Chi-Wang Shu, and Eitan Tadmor. Strong stability-preserving high-order time discretization methods. SIAM Rev., 43(1):89–112 (electronic), 2001.

[5] Amiram Harten. High resolution schemes for hyperbolic conservation laws. J. Comput. Phys., 49:357–393, 1983.

[6] Alexander Kurganov and Doron Levy. A third-order semidiscrete central scheme for conservation laws and convection-diffusion equations. SIAM J. Sci. Comput., 22(4):1461–1488 (electronic), 2000.

[7] Alexander Kurganov and Doron Levy. Central-upwind schemes for the Saint-Venant system. M2AN Math. Model. Numer. Anal., 36(3):397–425, 2002.

[8] Alexander Kurganov, Sebastian Noelle, and Guergana Petrova. Semidiscrete central-upwind schemes for hyperbolic conservation laws and Hamilton-Jacobi equations. SIAM J. Sci. Comput., 23(3):707–740 (electronic), 2001.

[9] Alexander Kurganov and Guergana Petrova. A second-order well-balanced positivity preserving central-upwind scheme for the Saint-Venant system. Commun. Math. Sci., 5(1):133–160, 2007.

[10] Alexander Kurganov and Eitan Tadmor. New high-resolution central schemes for nonlinear conservation laws and convection-diffusion equations. J. Comput. Phys., 160(1):241–282, 2000.

[11] R.J. LeVeque. Balancing source terms and flux gradients in high-resolution godunov methods: the quasi-steady wave-propagation algorithm. J. Comput. Phys., 146(2):346–365, 1998.

[12] Doron Levy, Gabriella Puppo, and Giovanni Russo. A third order central WENO scheme for 2D conservation laws. Appl. Numer. Math., 33(1-4):415–421, 2000.

[13] Haim Nessyahu and Eitan Tadmor. Nonoscillatory central differencing for hyperbolic conservation laws. J. Comput. Phys., 87(2):408–463, 1990.

[14] P. L. Roe. Approximate Riemann solvers, parameter vectors, and difference schemes. J. Comput. Phys., 43(2):357–372, 1981.

[15] Chi-Wang Shu and Stanley Osher. Efficient implementation of essentially nonoscillatory shock-capturing schemes. II. J. Comput. Phys., 83(1):32–78, 1989.

[16] Bram van Leer. Towards the ultimate conservative difference scheme. V. A second-order sequel to Godunov's method [J. Comput. Phys. **32** (1979), no. 1, 101–136]. J. Comput. Phys., 135(2):227–248, 1997.

[17] María Elena Vázquez-Cendón. Improved treatment of source terms in upwind schemes for the shallow water equations in channels with irregular geometry. J. Comput. Phys., 148(2):497–526, 1999.

Appendix

A Proof of Theorem 2.1

Proof:

(i) Starting with the initial conditions $u(x) = 0$ and $w(x) = W$ for all x, we fix a space scale Δx and the corresponding partition of the solution domain, $\{I_j\} := \{[x_{j-\frac{1}{2}}, x_{j+\frac{1}{2}}]\}$. We then define the cell averages of the conserved quantities in the modified shallow water model, (2.1), as

$$\overline{A}_j^T := \sigma_j \, \overline{w}_j = \sigma_j \, W, \tag{A.1}$$

and

$$\overline{Q}_j := \left(\overline{A}_j - \frac{1}{2}\sigma_j \left(B(x_{j+\frac{1}{2}}) + B(x_{j-\frac{1}{2}}) \right) \right) \overline{u}_j \equiv 0. \tag{A.2}$$

The reconstructed point values of w and Q, clearly satisfy $w^{\pm}_{j\pm\frac{1}{2}} = W$ and $Q^{\pm}_{j\pm\frac{1}{2}} = 0$, thus the values of the water height, (2.19), and those of the bottom topography at the cell interfaces, $B(x_{j\pm\frac{1}{2}})$, satisfy

$$h^-_{j+\frac{1}{2}} - h^+_{j-\frac{1}{2}} = - \left(B(x_{j+\frac{1}{2}}) - B(x_{j-\frac{1}{2}}) \right).$$

In view of this, the first component of the numerical fluxes $H_{j+\frac{1}{2}}$ in (2.8) reads

$$-\frac{H^{(1)}_{j+\frac{1}{2}} - H^{(1)}_{j-\frac{1}{2}}}{\Delta x} = -\frac{1}{2\Delta x} \left[a_{j+\frac{1}{2}}\sigma_{j+\frac{1}{2}} \left(w^+_{j+\frac{1}{2}} - w^-_{j+\frac{1}{2}} \right) - a_{j-\frac{1}{2}}\sigma_{j-\frac{1}{2}} \left(w^+_{j-\frac{1}{2}} - w^-_{j-\frac{1}{2}} \right) \right] \equiv 0. \tag{A.3}$$

That is,

$$\frac{d}{dt}\overline{A}^T_j(t) = 0 \qquad \Rightarrow \qquad \overline{A}^T_j(t + \Delta t) = \overline{A}^T_j(t), \tag{A.4}$$

which allows us to recover $\overline{w}_j(t + \Delta t) = W$ exactly from (A.1).

Noting that, according to (2.19), $h^+_{j+\frac{1}{2}} = h^-_{j+\frac{1}{2}} =: h_{j+\frac{1}{2}}$, the second component of the numerical flux amounts to (2.20), and since (2.12) holds, it is balanced by (2.23)-(2.24), therefore

$$\frac{d}{dt}\overline{Q}_j(t) = 0 \qquad \Rightarrow \qquad \overline{Q}_j(t + \Delta t) = \overline{Q}_j(t) = 0, \tag{A.5}$$

and $u_j(t + \Delta t) \equiv 0$ is also recovered exactly. □

(ii) We begin by writing explicitly the cell average $A^T_j(t + \Delta t)$ when the system (2.8) is evolved with *forward Euler's* ODE solver,

$$\overline{A}^T_j(t + \Delta t) = \overline{A}^T_j(t) - \lambda \left[H^{(1)}_{j+\frac{1}{2}}(t) - H^{(1)}_{j-\frac{1}{2}}(t) \right], \tag{A.6}$$

where $\lambda = \Delta t/\Delta x$. This amounts to

$$\begin{aligned} \overline{A}^T_j(t + \Delta t) \; = \overline{A}^T_j(t) \quad - \quad & \frac{\lambda}{2} \left[\left(Q^+_{j+\frac{1}{2}} + Q^-_{j+\frac{1}{2}} \right) - a_{j+\frac{1}{2}} \left(A^{T,+}_{j+\frac{1}{2}} - A^{T,-}_{j+\frac{1}{2}} \right) \right. \\ & \left. - \left(Q^+_{j-\frac{1}{2}} + Q^-_{j-\frac{1}{2}} \right) + a_{j-\frac{1}{2}} \left(A^{T,+}_{j-\frac{1}{2}} - A^{T,-}_{j+\frac{1}{2}} \right) \right], \end{aligned} \tag{A.7}$$

(where all the terms on the right hand side are understood to be evaluated at time t). Using $Q^{\pm}_{j\pm\frac{1}{2}} = \sigma^{\pm}_{j\pm\frac{1}{2}} h^{\pm}_{j\pm\frac{1}{2}}$, we write

$$\begin{aligned}
\overline{A}^T_j(t+\Delta t) \;=\overline{A}^T(t) \;+\; \frac{\lambda}{2}\Big[&\Big(a_{j+\frac{1}{2}}\sigma_{j+\frac{1}{2}} - u^+_{j+\frac{1}{2}}\sigma^+_{j+\frac{1}{2}}\Big)h^+_{j+\frac{1}{2}} + \Big(a_{j-\frac{1}{2}}\sigma_{j-\frac{1}{2}} + u^-_{j-\frac{1}{2}}\sigma^-_{j-\frac{1}{2}}\Big)h^-_{j-\frac{1}{2}} \\
&+\; a_{j+\frac{1}{2}}\sigma_{j+\frac{1}{2}}B(x_{j+\frac{1}{2}}) \;+\; a_{j-\frac{1}{2}}\sigma_{j-\frac{1}{2}}B(x_{j-\frac{1}{2}})\Big] \\
-\;\frac{\lambda}{2}\Big[&\Big(a_{j+\frac{1}{2}}\sigma_{j+\frac{1}{2}} + u^-_{j+\frac{1}{2}}\sigma^-_{j+\frac{1}{2}}\Big)h^-_{j+\frac{1}{2}} + \Big(a_{j-\frac{1}{2}}\sigma_{j-\frac{1}{2}} - u^+_{j-\frac{1}{2}}\sigma^+_{j-\frac{1}{2}}\Big)h^+_{j-\frac{1}{2}} \\
&+\; a_{j+\frac{1}{2}}\sigma_{j+\frac{1}{2}}B(x_{j+\frac{1}{2}}) \;+\; a_{j-\frac{1}{2}}\sigma_{j-\frac{1}{2}}B(x_{j-\frac{1}{2}})\Big].
\end{aligned} \tag{A.8}$$

The terms involving $\sigma_{j\pm\frac{1}{2}}B(x_{j\pm\frac{1}{2}})$ on the right hand side cancel, and since $a_{j\pm\frac{1}{2}}\sigma_{j\pm\frac{1}{2}} \geq |u^{\pm}_{j\pm\frac{1}{2}}|\,\sigma^{\pm}_{j\pm\frac{1}{2}}$, (2.30), and $h^{\mp}_{j\pm\frac{1}{2}} \geq 0$, the *CFL* restriction (2.35) allows us to write

$$\overline{A}^T_j(t+\Delta t) \;\geq\; \overline{A}^T_j(t) - \frac{1}{2}\sigma_j\left(h^-_{j+\frac{1}{2}} + h^+_{j-\frac{1}{2}}\right) = \frac{1}{2}\sigma_j\left(B(x_{j+\frac{1}{2}}) + B(x_{j-\frac{1}{2})})\right), \tag{A.9}$$

from where (2.36) follows. And since the Runge-Kutta solver (2.31) – (2.32) consists of a convex combination of forward Euler steps, the result holds when this evolution routine is employed. □